

# Enhancement of adhesion strength in viscoelastic unsteady contacts

C. Mandriota,<sup>1</sup> N. Menga,<sup>1,2</sup> and G. Carbone<sup>1,3</sup>

<sup>1</sup>*Department of Mechanics, Mathematics and Management,  
Politecnico of Bari, Via Orabona, 4, 70125, Bari, Italy*

<sup>2</sup>*Corresponding author. Email: nicola.menga@poliba.it*

<sup>3</sup>*CNR - Institute for Photonics and Nanotechnologies U.O.S. Bari,  
Physics Department "M. Merlin", via Amendola 173, 70126 Bari, Italy*

## Abstract

We present a general energy approach to study the unsteady adhesive contact of viscoelastic materials. Under the assumption of infinitely short-range adhesive interactions, we exploit the principle of virtual work to generalize Griffith's local energy balance at contact edges to the case of a non-conservative (viscoelastic) material, subjected to a generic contact time-history. We apply the proposed energy balance criterion to study the approach-retraction motion of a rigid sphere in contact with a viscoelastic half-space. A strong interplay between adhesion and viscoelastic hysteretic losses is reported which can lead to strong increased adhesion strength, depending on the loading history. Specifically, two different mechanisms are found to govern the increase of pull-off force during either approach – retraction cycles and approach – full relaxation – retraction tests. In the former case, hysteretic losses occurring close to the circular perimeter of the contact play a major role, significantly enhancing the energy release rate. In the latter case, instead, the pull-off enhancement mostly depends on the glassy response of the whole (bulk) material which, triggered by the fast retraction after relaxation, leads to a sort of ‘frozen’ state and results in a flat-punch-like detachment mechanism (i.e., constant contact area). In this case, the JKR theory of adhesive contact cannot be invoked to relate the observed pull-off force to the effective adhesion energy, i.e. the energy release rate  $G$ , and strongly overestimates it. Therefore, a rigorous mathematical procedure is also proposed to correctly calculate the energy release rate in viscoelastic dissipative contacts.

Keywords: viscoelasticity, adhesion, retraction, crack propagation, hysteresis

## I. INTRODUCTION

The Johnson, Kendall and Roberts (JKR) seminal study [1] on adhesive elastic spheres is a milestone in the field of adhesive contact mechanics of soft elastic solids. Moving from the assumption of infinitely short-range adhesive interactions and exploiting the Griffith energy balance criterion [2], the JKR model was able to provide results in perfect agreement with experiments thus paving the way for modelling a wide class of elastic adhesive smooth [7, 67] and rough contacts [8–10], as well as other applications such as the peeling of thin tapes [84, 85]. By following the same energy balance principle, the influence of tangential stresses in sliding adhesive contacts can be investigated [11, 12], as well as the effect of thickness of the elastic coatings [52, 73], and of different geometries and boundary conditions [13–16]. As long as the Tabor parameter is sufficiently large [6], the energy balance approach has the advantage to correctly model adhesive contacts only requiring a few quantities as inputs: the Young modulus and Poisson ratio of the isotropic elastic material, and the adhesion energy per unit area  $\Delta\gamma$ . The latter, in particular, has a very simple definition in terms of macroscopic quantities and can be easily measured through reliable experimental procedures, regardless of the detailed interfacial gap dependence of the molecular interactions. Hence, once the experimental data are acquired using, for instance, micro-scale optical microscopy [4], scratch tests [3], peeling processes [5], or macro-scale spherical indentation-retraction tests [79, 80],  $\Delta\gamma$  can be easily derived by fitting them with the corresponding elastic contact model.

Nonetheless, the JKR contact theory falls short in tackling adhesive contact problems of rubber-like materials when quasi-static conditions are not ensured, as clearly indicated by several experimental evidences. This is often ascribed to the intrinsic viscoelastic response of rubber, whose non-conservative nature makes Griffith’s energy balance no longer valid. Indeed, a velocity-dependent response is experimentally observed, e.g. in rolling contacts of natural rubber [86] with respect to the real adhesion force. Similarly, JKR-like dynamic tests on siloxane and acrylic elastomers reveal velocity-dependent hysteresis, for both approach-retraction [21, 34] and oscillating [18] tests, with highly enhanced effective adhesion energy reported during retraction. Experiments have also been devoted to investigate the effect of dwell time before retraction [87, 88], preload [22, 30], and micro vibration during retraction [23, 89, 90]. Although some attempts have been made to predict the retraction behavior by introducing velocity-dependent (usually, power law) adhesion energy terms [20, 21, 33, 76], the overall effect of viscoelasticity in adhesive contacts is still not fully understood. Indeed, the interplay between viscoelasticity and adhesion in unsteady contacts is a complex phenomenon, affected by the overall loading history and not only by the instantaneous crack speed at the contact boundary, as demonstrated by several experimental studies highlighting the effect of the dwell time before retraction [87, 88], the preload [22, 30], and the imposed micro vibration during retraction [23, 89, 90]. More importantly, variational approaches to viscoelastic continuum mechanics [58–60] usually result in greater complexity compared to corresponding elastic cases, therefore discouraging the attempts to adapt JKR approach to viscoelastic contacts. As a consequence, the common approach to investigate adhesive viscoelastic contacts is to assume that viscoelastic losses occur very locally at the boundary of the contact, while in the bulk the material response is governed by the soft elastic modulus [21, 25, 33, 36]. This assumption, known as the ‘small-scale viscoelasticity’ hypothesis, has been shown to be very effective and accurate for systems which do not present any specific length scale, e.g. a semi-infinite crack propagating in infinite viscoelastic sheet, or for contact

problems where the characteristic size  $a$  of the contact is  $a \gg V\tau$  where  $V$  is a characteristic velocity and  $\tau$  the relaxation time of the material. However, when the above conditions are not fulfilled, recent studies [17, 37] have proved that the small-scale viscoelasticity assumption leads to significant qualitative and quantitative errors, which are mainly related to the neglected bulk viscoelastic dissipation. In the attempt to deal also with these cases, most of the existing studies exploit local force equilibrium where the contacting surface are discretized in particles or elements which interact with the corresponding particles/elements of the counter surface through local forces, derived by gap-dependent potentials, e.g.  $m-n$  potentials [32], as the Lennard-Jones (LJ) law [27, 28, 35, 68, 71], exponentially short-range laws [31, 69], and cohesive-zone models specifically designed for contact [24, 29, 40, 78] and fracture mechanics [42, 43] problems. However, as clearly observed by Persson [63] and Greenwood [70], the contact behavior is weakly affected by the specific law implemented to describe the interfacial adhesive interaction, provided that the range of microscopic gap dependent law is much shorter than any other length scale involved in the problem. This suggests that most of the phenomena in viscoelastic contacts can be captured by general energy equilibrium, as indeed shown at least for the case steady-state viscoelastic sliding contacts in Ref. [17, 37].

The present study generalizes the adhesive viscoelastic contact theory presented in [17, 37] to the case of unsteady conditions (dynamic loading), thus formally deriving a general Griffith-like criterion for viscoelastic contacts and unsteady crack propagation in hysteretic materials (e.g. delayed fracture of soft polymers). We derive the energy balance by relying on the D'Alembert principle of virtual works: the variation of adhesion energy due to a virtual change of the contact area (the Lagrangian coordinate) must be precisely balanced by the virtual work of internal stresses. Our findings are in perfect agreement with aforementioned experimental results and LJ based numerical calculations [35, 68, 71, 77], and clearly indicate that viscoelasticity plays a major role in affecting adhesion enhancement depending on the specific loading-history. Our theoretical approach also provides very profound insights into the physical mechanisms governing experimentally observed phenomena such as the enhancement of pull-off force during fast retraction [19, 21, 22, 26], the hysteresis during the approach-retraction cycle [21, 34], and effective contact stiffness during high frequency oscillations [89, 90]. Overall, the present theory may be of interest to quantify the effects of adhesion in several engineering applications involving viscoelastic polymeric materials such as, for instance, structural adhesives [44, 45], pressure-sensitive adhesives [46], protective coatings [47], bioinspired adhesives [48, 49], orthopedic applications [50, 51], micro-electro-mechanical systems [53, 54], micro-manipulations and micro-assembly [55, 56].

## II. FORMULATION

We consider the adhesive contact between a linear viscoelastic half-space and a rigid sphere of radius  $R$  subjected to a time-varying rigid normal displacement  $u_0(t)$ , as shown in Fig 1. Following [38, 39], the normal displacement field  $u(\mathbf{x}, t)$  of the viscoelastic half-space surface is given by

$$u(\mathbf{x}, t) = J(0) \int dx_1^2 \mathcal{G}(\mathbf{x} - \mathbf{x}_1) \sigma(\mathbf{x}_1, t) + \int_{-\infty}^t dt_1 \dot{J}(t - t_1) \int dx_1^2 \mathcal{G}(\mathbf{x} - \mathbf{x}_1) \sigma(\mathbf{x}_1, t_1) \quad (1)$$

where  $\mathbf{x}$  is the in-plane position vector,  $t$  is the time variable,  $\sigma(\mathbf{x}, t)$  is the interfacial normal stress distribution,  $J(t)$  is the viscoelastic creep function, and  $\mathcal{G}(\mathbf{x}) = (1 - \nu^2)|\mathbf{x}|^{-1}/\pi$ .

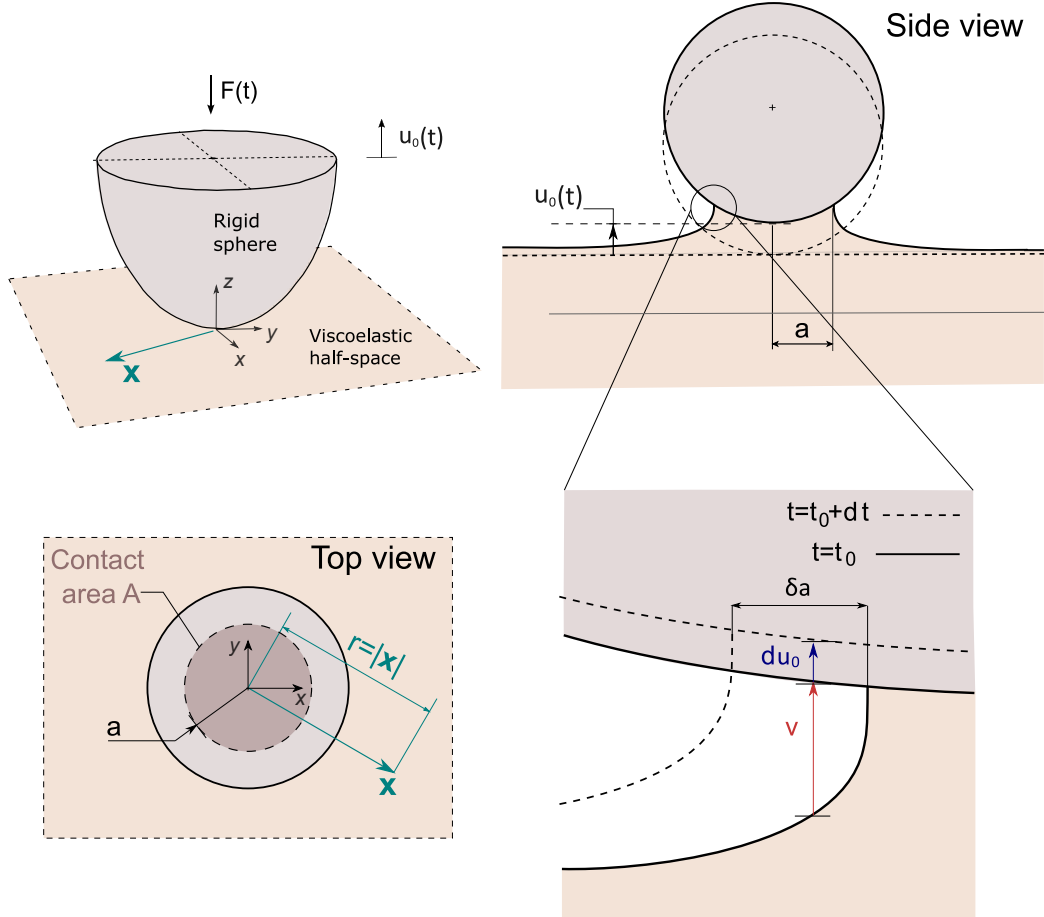


FIG. 1: The schematic of the adhesive contact between a viscoelastic half-space and a rigid sphere, with time-varying normal rigid displacement  $u_0(t)$ . The inset represents the virtual component  $v$  of the local displacement  $v + du_0$  close to the contact edge associated with the contact area variation  $\delta a$  and indenter rigid displacement  $du_0$ .

As we are considering the approach/retraction of a sphere, the problem at hand, which belong to the class of mixed value problems, is axisymmetric, i.e., at each time step  $t$  all quantities depend only on the distance  $r = |\mathbf{x}|$  from the contact center (see Fig. 1). Under the assumption of infinitely short range interfacial adhesive interactions, outside the circular contact region of radius  $a(t)$  the surface stresses must vanish, i.e.  $\sigma(r, t) = 0$  for  $r > a(t)$ , whilst within the contact region the surface displacement field is prescribed, i.e.  $u(r, t) = s(r, t)$  for  $r \leq a(t)$ , with  $s(r, t) = u_0(t) + r^2/(2R)$  being the spherical indenter surface at time  $t$ . We also define the local interfacial gap as  $g(r, t) = s(r, t) - u(r, t)$ , so that  $g(r, t) = 0$  for  $r \leq a(t)$ . Note that, given a value of the rigid normal displacement  $u_0(t)$ , Eq. (1) cannot be solved as the contact radius  $a(t)$  is not known, and an additional closure equation is needed to solve the problem. In the case of adhesiveless contacts, the closure condition is simply that the interfacial contact stress must vanish at the boundary of the contact area; however, for adhesive contacts, tensile stress can also be sustained, and an energy based condition should be identified. In virtue of the principle of virtual works (PVW), the equilibrium configuration at time  $t$  requires that the work of external forces  $\delta L_E$  due to an admissible virtual displacements field equates the work of internal

stresses  $\delta L_I$  due to the corresponding compatible virtual strain field. Since the virtual displacements field  $\delta \mathbf{v}(r, z, t)$  must only satisfy the boundary conditions at time  $t$  (i.e., the kinematic constraints), we have  $\delta \mathbf{v}(x, z, t) = 0$  within the contact region, i.e. where the time-dependent constraint  $u(r, t) = s(r, t)$  is prescribed. Then, neglecting body forces, at equilibrium we have

$$\delta L_I = \int_W \sigma_{ij} \delta \varepsilon_{ij} dV = \int_{\partial W} \sigma \cdot \delta \mathbf{v} dA = \delta L_E \quad (2)$$

for any admissible virtual displacement  $\delta \mathbf{v}$  and its associated internal strain tensor  $\delta \varepsilon_{ij}$ , where  $\sigma$  is the surface stress field, and  $\sigma_{ij}$  is the internal stress tensor.

For the contact problem represented in Fig. 1, we assume a virtual variation (i.e., at fixed time  $t$ ) of the contact configuration so that the contact radius increases from  $a(t)$  to  $a(t) + \delta a$ . Consequently, the asymptotic surface displacements at the contact edge [i.e., for  $|r - a(t)| \ll a(t)$ ] changes by the quantity  $v^-(r) = g[r \geq a(t), t]$ . This can be described by the virtual displacement process  $v(r, \eta) = v^-(r)H(\eta)$ , where  $H(\eta)$  is the unit step function, and  $\eta$  is the process parameter spanning the entire real axis. Therefore, at each step of the process, the virtual normal displacement  $\delta v(r, \eta)$  obeys the equation

$$\delta v(r, \eta) = \frac{\partial v}{\partial \eta} d\eta = v^-(r) \delta(\eta) d\eta \quad (3)$$

where  $\delta(\eta)$  is the Dirac delta function. Similarly the asymptotic stress distribution  $\sigma_a$  close to the boundary of the contact area [i.e., for  $|a(t) - r| \ll a(t)$ ] has the form  $\sigma_a[a(t) - r, t] = \sigma[r < a(t), t]$ . Therefore, during the virtual displacement process governed by the parameter  $\eta$ , the corresponding asymptotic surface stresses are given by

$$\sigma(r, \eta) = \sigma^+(r)H(\eta) \quad (4)$$

where  $\sigma^+(r) = \sigma_a[a(t) + \delta a - r, t]$ . It follows that during the entire  $\eta$ -governed process, the total virtual work  $(\delta L_I)_T$  of internal stresses due to the contact radius virtual variation from  $a(t)$  to  $a(t) + \delta a$  can be calculated as

$$(\delta L_I)_T = 2\pi \int_a^{a+\delta a} r dr \int_{-\infty}^{\infty} d\eta \sigma(r, \eta) \frac{\partial v}{\partial \eta} = 2\pi \int_a^{a+\delta a} r dr \sigma^+(r) v^-(r) \int_{-\infty}^{\infty} d\eta H(\eta) \delta(\eta) \quad (5)$$

and, recalling that  $\int_{-\infty}^{\infty} d\eta H(\eta) \delta(\eta) = 1/2$ , we finally get

$$(\delta L_I)_T = \pi a \int_a^{a+\delta a} dr \sigma^+(r) v^-(r) \quad (6)$$

The virtual (external) work of adhesive forces during the entire displacement process is instead

$$(\delta L_E)_T = 2\pi \Delta \gamma a \delta a \quad (7)$$

Thus, exploiting Eq. (2) at each single step of the displacement process, the energy balance gives

$$(\delta L_I)_T = (\delta L_E)_T \quad (8)$$

which, using Eqs. (6,7), can be rewritten as

$$\frac{1}{2\delta a} \int_a^{a+\delta a} dr \sigma^+(r) v^-(r) = \Delta \gamma \quad (9)$$

Eq. (9) represents the generalization of the Griffith fracture criterion for unsteady contacts and holds true for both elastic and viscoelastic materials. The positive quantity  $\delta a$  should be chosen of the same order of magnitude of the so-called ‘process zone’ at the contact edges [61]. Specific cases, such as thin pressure-sensitive membrane [91, 92], might require replacing in Eq. (9) the adhesion energy  $\Delta\gamma$  with a modified energy of adhesion which depends on both the propagation speed of the crack tip and temperature of the process zone. The quantity  $\delta a$  or equivalently the length of the process zone is an additional (short) length scale, whose choice does not affect the physical qualitative behavior of the viscoelastic contact problem at hand, as it only shifts the frequency of the local excitation occurring close to the boundary of the contact. Notably, Eq. 9 holds true also for the case of steady state viscoelastic adhesive contact and is formally the same as that derived in [17, 37] following a different argument.

### III. RESULTS AND DISCUSSION

We consider a viscoelastic material with a single relaxation-time  $\tau$  and relaxation function given by

$$G(t) = \mathcal{H}(t) \{E_\infty + (E_0 - E_\infty) [1 - \exp(-t/\tau)]\} \quad (10)$$

also corresponding to the creep function given by

$$J(t) = \mathcal{H}(t) \left\{ \frac{1}{E_\infty} + \left( \frac{1}{E_0} - \frac{1}{E_\infty} \right) \left[ 1 - \exp\left(-\frac{E_0}{E_\infty} \frac{t}{\tau}\right) \right] \right\} \quad (11)$$

where  $E_0$ , and  $E_\infty$  are the low-frequency and very high-frequency viscoelastic moduli of the material respectively. Real rubber-like materials usually present more complex rheology with several relaxation times, so that a Prony series description of the relaxation-creep functions is required; however, qualitative physical insights can still be drawn with a single-relaxation time.

Results are shown in terms of the following dimensionless quantities:  $\tilde{p} = (1 - \nu^2) p / (\pi E_0)$ ,  $\tilde{u} = u/R$ ,  $\tilde{\gamma} = (1 - \nu^2) \Delta\gamma / (\pi E_0 R)$ ,  $\tilde{F} = (1 - \nu^2) F / (\pi E_0 R^2)$ ,  $\tilde{V} = V\tau/R$ ,  $\tilde{u}_0 = u_0/R$ ,  $\tilde{\Delta} = \Delta/R$ ,  $\tilde{t} = t/\tau$ ,  $\tilde{r} = r/R$ ,  $\tilde{a} = a/R$ , with  $p(r, t) = -\sigma(r, t)$  being the contact pressure,  $\Delta = -u_0$  the contact penetration, and  $F = \int d^2x p(r, t)$  the normal compressive applied force. In our calculations, we set unless  $\delta\tilde{a} = 0.013$ ,  $\tilde{\gamma} = 1.6 \times 10^{-4}$  (except in Fig. 7), and  $E_\infty/E_0 = 10$ . We also define the normal approach-retraction speed of the sphere as  $V = |\dot{u}_0| = \left| \dot{\tilde{\Delta}} \right|$ , where the superposed dot ‘.’ stands for the time derivative. Notice that, unless differently specified,  $V$  is the controlled parameter in our calculations.

Firstly, we focus on the effect of the imposed indenter dimensionless speed  $\tilde{V}$  in approach-retraction (A-R) cycles with vanishing dwell time  $\tilde{t}_d = t_d/\tau \rightarrow 0$ , as reported in Fig. 2. Calculations are initialized assuming an instantaneous jump into contact at  $\tilde{\Delta} = 0$ . Therefore, regardless of  $\tilde{V}$ , the system response is purely elastic and follows the adhesive JKR solution with the elastic modulus given by  $E_\infty$ . At very low A-R speed (see results for  $\tilde{V} = 2 \times 10^{-5}$ ), the loading process is sufficiently slow to allow for full relaxation of the viscoelastic material, and the soft elastic JKR response with low frequency modulus  $E_0$  is recovered during both approach and retraction (i.e., no hysteresis is observed). Similarly, at very high speed (i.e.,  $\tilde{V} \gg 1$ ), the material behaves as a stiff elastic body and the glassy elastic JKR response occurs, with vanishing hysteresis during the loading-unloading cycles. As expected, in both

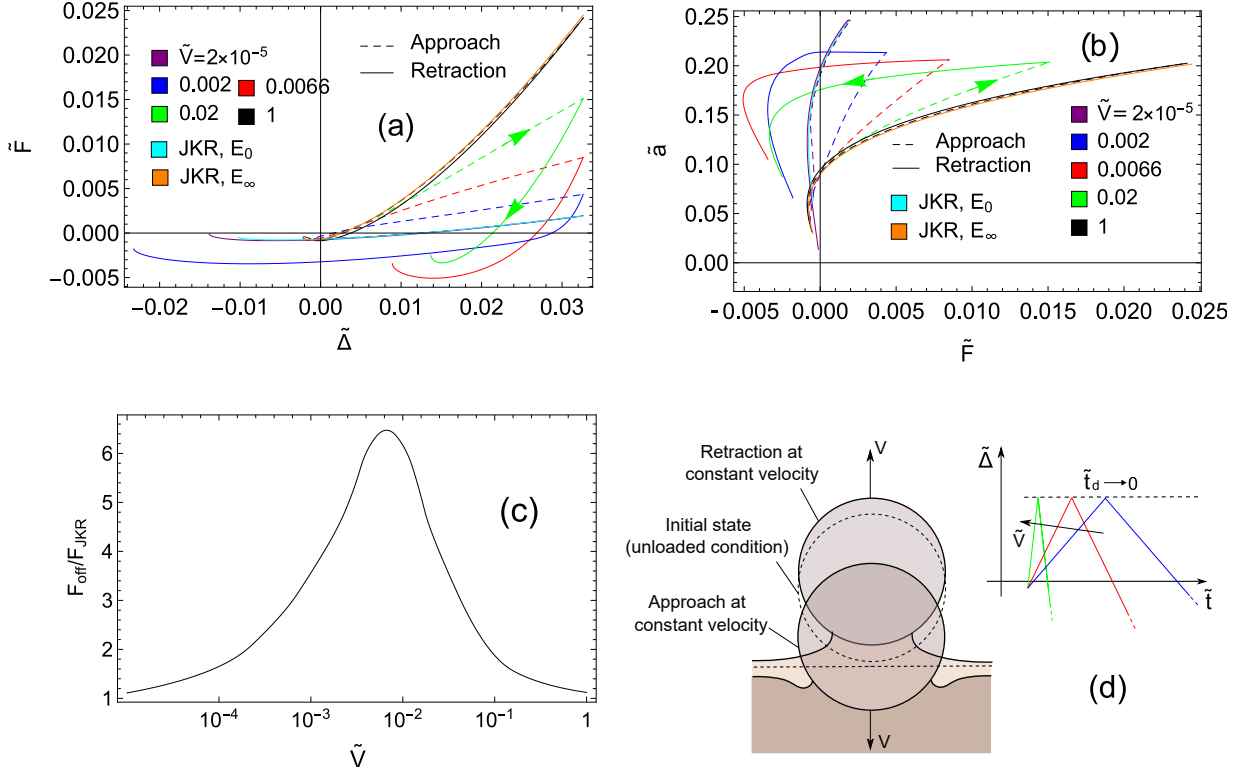


FIG. 2: Approach-retraction cycles at different dimensionless sphere velocity  $\tilde{V}$ . Dashed and solid lines refer, respectively, to indentation and retraction, until pull-off occurs. (a) The dimensionless applied load  $\tilde{F}$  vs. the dimensionless indentation depth  $\tilde{\Delta}$ . (b) The dimensionless contact radius  $\tilde{a}$  vs. the dimensionless applied load  $\tilde{F}$ . The JKR elastic curves corresponding to moduli  $E_0$  and  $E_\infty$  are reported for comparison. (c) The viscoelastic-elastic pull-off force ratio  $F_{\text{off}}/F_{\text{JKR}}$  as function of the sphere velocity. (d) The process schematic and the qualitative dimensionless penetration  $\tilde{\Delta}$  time-history. Results are shown for  $\tilde{\gamma} = 1.6 \times 10^{-4}$ ,  $E_\infty/E_0 = 10$ .

cases the maximum tensile load (i.e. the pull-off force) takes the same value, independently of the value of the effective elastic modulus. Nonetheless, results in Fig. 2 clearly show that viscoelastic dissipation induces large adhesive hysteresis in A-R cycles at intermediate values of  $\tilde{V}$ . These findings are in agreement with experimental results [21, 22, 26, 30] and show that, during retraction, the system is able to withstand significantly larger tensile loads compared to the elastic case, as also shown in [20, 22, 30, 33, 34]. A closer look at Fig. 2(a) reveals that the maximum tensile stress (pull-off) can either occur at larger retraction distances compared to the elastic JKR and, for relatively large A-R speeds, even at positive penetration  $\Delta > 0$ , in agreement with experimental results [19, 26]. In the latter case, while approaching, the material has not yet reached the viscoelastic glassy response. However, when the indenter motion is reversed (i.e., the speed jumps from  $\dot{\Delta} = V$  to  $\dot{\Delta} = -V$ ), the glassy behavior is triggered (with elastic modulus  $E_\infty$ ) and, since retraction occurs sufficiently fast, viscoelastic dissipation prevents the material from relaxing and detachment occurs at positive values of penetration  $\Delta$ , with contact area and tensile load much larger than the elastic case.

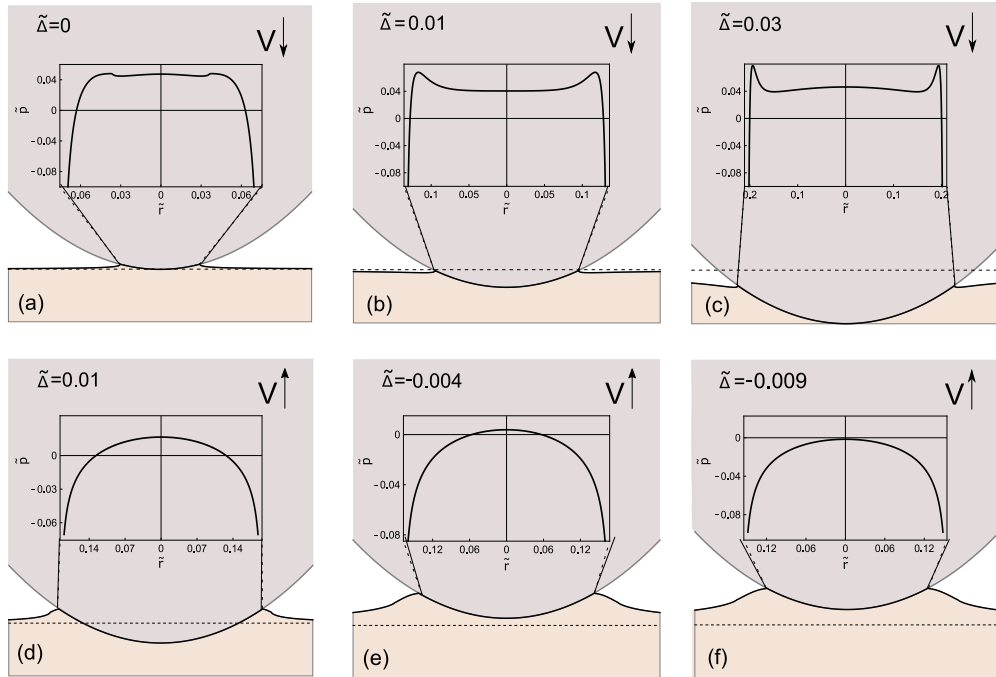


FIG. 3: The deformed contact configuration during indentation (a-c) and retraction (d-f) at dimensionless sphere speed  $\tilde{V} = 0.002$  (i.e, blue line in Fig.2) for different values of the dimensionless penetration  $\tilde{\Delta}$ . The inset shows the corresponding dimensionless contact pressure distribution  $\tilde{p}$ . Results are shown for  $\tilde{\gamma} = 1.6 \times 10^{-4}$ ,  $E_{\infty}/E_0 = 10$ .

Fig. 3 reports the surface displacement and the pressure distributions during an approach-retraction cycle at the given dimensionless speed  $\tilde{V} = 0.002$ . Focusing on the approach stage, beside the expected adhesion-induced square root singularity at the contact boundary, the interfacial pressure distribution also presents a positive annular peak close to the advancing circular perimeter of the contact area. A similar trend has been reported for viscoelastic adhesiveless approaching contacts in Ref. [39] and at the leading edge of rolling (or frictionless sliding) viscoelastic contacts [17, 38, 72, 75]. Moreover, during the early stages of the retraction process, the size of the contact area negligibly changes, and it drops only once the maximum tensile load is reached, as also confirmed by experimental observation [20–22, 33]. Noteworthy, during the retraction stage, the annular pressure peak disappears, and the adhesion-induced pressure singularity is associated with a trumpet-like opening crack shape, as predicted by de Gennes [61].

Results in Fig. 2 have shown that a viscoelastic-induced enhancement of the pull-off force can be observed at intermediate approach-retraction speeds, i.e. when the material has not yet fully entered the glassy state during the approach stage. Hence, one may guess that the enhancement of pull-off force or, equivalently, of the adhesion strength should be even more amplified if the retraction stage is allowed to begin, at finite speed, immediately after an extremely slow approach stage. This correspond to retraction from fully relaxed conditions at fixed positive penetration  $\Delta > 0$  (dwell time  $t_d \rightarrow +\infty$ ), which is what we report in Fig. 4 for different dimensionless retraction speeds  $\tilde{V}$ . Specifically, retraction starts from point B at given dimensionless penetration  $\tilde{\Delta}_B = 0.032$  which, as predicted by the fully relaxed elastic JKR solution (i.e., with elastic modulus  $E_0$ ), corresponds to dimensionless contact

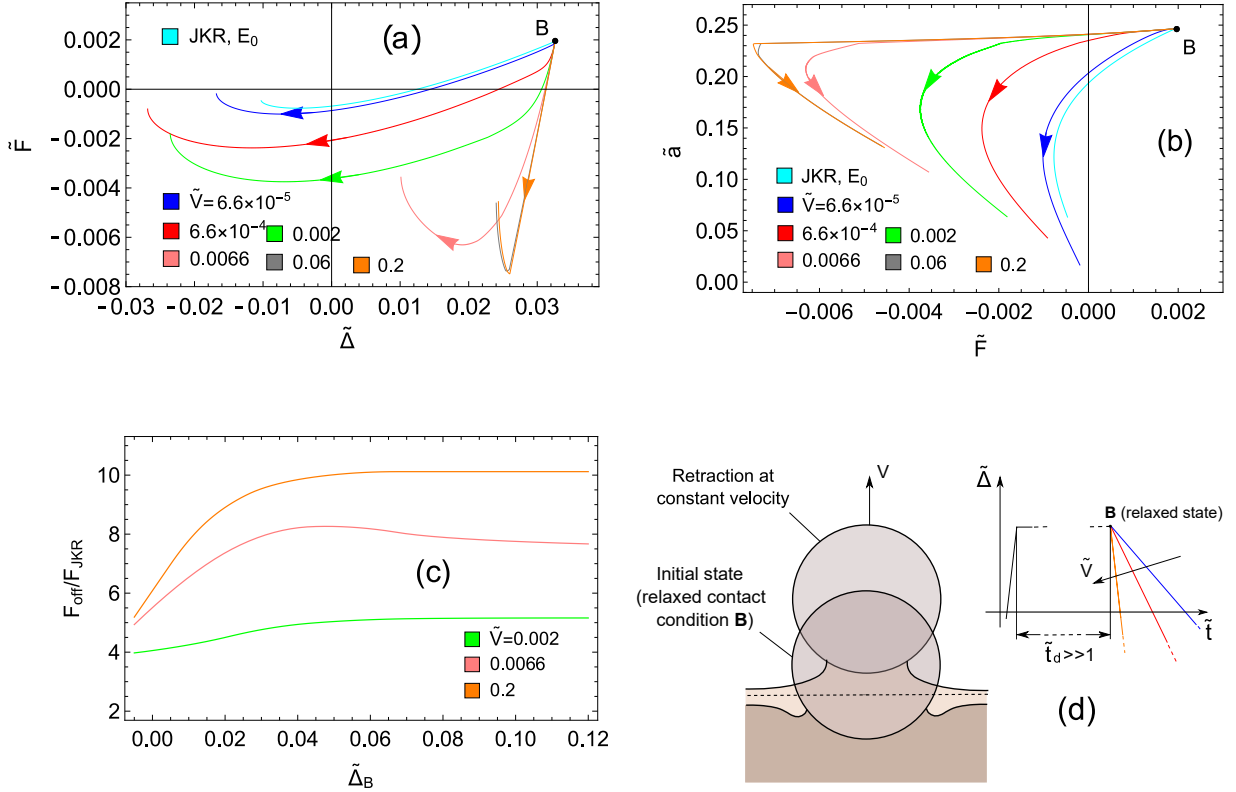


FIG. 4: Sphere retraction at different dimensionless speed  $\tilde{V}$  from fully relaxed conditions (point B, with  $\tilde{\Delta}_B = 0.032$ ). (a) The dimensionless applied load  $\tilde{F}$  vs. the dimensionless indentation depth  $\tilde{\Delta}$ . (b) The dimensionless contact radius  $\tilde{a}$  vs. the dimensionless applied load  $\tilde{F}$ . (c) The normalized pull-off force  $F_{\text{off}}/F_{\text{JKR}}$  vs. the initial dimensionless penetration  $\tilde{\Delta}_B$ . (d) The process schematic and qualitative time-history. Results are shown for  $\tilde{\gamma} = 1.6 \times 10^{-4}$ ,  $E_\infty/E_0 = 10$ .

radius  $\tilde{a}_B = 0.245$  and dimensionless normal load  $\tilde{F}_B = 1.87 \times 10^{-3}$ . During retraction, given a finite speed  $V$ , the contact penetration is  $\Delta = \Delta_B - H(t)Vt$ , where  $H(t)$  is the unit step function, and the retraction speed instantaneously jumps from 0 to  $-V$  at  $t = 0$  (notice,  $\dot{\Delta} = -H(t)V$ ). Therefore, at the early stages of the retraction process (i.e., for  $t \ll \tau$ ), the material response is elastic, with modulus  $E_\infty$ . Now, considering that: (i) a decrease of the contact area can only occur if the condition  $g(r, t) \geq 0$  is fulfilled, (ii) a certain time or, equivalently, a certain retraction distance is required before enough elastic energy is stored into the system, and (iii) a reduction of the contact area can only take place if the release of mechanical plus elastic energy is enough to compensate the change of adhesion energy, one concludes that during the initial stages of the retraction process the contact area will remain almost constant in a, say, ‘frozen’ state. When this happens the relation between the applied load  $F$  and the penetration  $\Delta$  must obey the flat-punch linear relation [6, 41]. Force-penetration linearity is indeed observed in Fig. 4 during the initial stages of retraction, regardless of the given finite speed  $V$ , and a similar behavior is also observed in temperature controlled systems [74], when the deformed material is cooled below the glass transition temperature  $T_g$  resulting in an almost ‘frozen’ contact shape. Provided that the material relaxation process has not yet started at detachment (i.e., the

retraction velocity is sufficiently high), the pull-off force  $F_{\text{off}}$  is much larger than the JKR prediction  $F_{\text{JKR}}$ , i.e.  $F_{\text{off}} > F_{\text{JKR}} = 3\Delta\gamma\pi R/2$ . As a consequence, we conclude that during fast retraction: (i) the material is in the glassy state hence, at pull-off the energy release rate  $G = K_I^2/(2E_\infty^*)$  with  $E_\infty^* = E_\infty(1 - \nu^2)$  must be necessarily equal to the adhesion energy per unit area, i.e.  $G = \Delta\gamma$  (the material is not tougher and no enhancement of the effective energy of adhesion occurs- see also Sec. III A), (ii) the force - penetration and the force - area curves are significantly different from JKR predictions, (iii) the pull-off force cannot be predicted by JKR theory. Therefore, any experimental/numerical estimation of the effective adhesion energy at high speed pull-off through JKR is inappropriate [25, 26, 33, 36, 68, 71]. Conversely, during slow retraction the material has enough time to partially relax. As a consequence, the maximum tensile force decreases compared to the value predicted by the aforementioned arguments and monotonically diminishes with decreasing  $V$ , eventually reaching the elastic JKR value for extremely slow retraction process. Contact stickiness and toughness are related to the minimum (negative) value of  $\Delta$  before pull-off, as described in [16, 17, 37, 73]. In this regard, we note that for very small values of  $V$  the soft elastic JKR limit is recovered, but, at intermediate values of  $V$ , a significantly larger elongations before pull-off is observed, compared to the elastic case. This happens when hysteretic viscoelastic losses occur only close to the circular boundary of the contact (small-scale viscoelasticity), where the material is excited on a time scale of order  $\rho/|\dot{a}| \approx \rho/V \approx \tau$ , where  $\rho \ll R$  is the radius of curvature of the contact adhesive neck. In such conditions, the bulk of the material is instead excited on time scales of order  $R/V > \tau$ , thus behaving as a soft elastic material with modulus  $E_0$ . In such ‘small-scale viscoelasticity’ regime the energy release rate increases (as better reported in Sec. III A), and the load-penetration and load-area curves are well approximated by the JKR predictions, provided that the adhesion energy  $\Delta\gamma$  is replaced by an effective value  $\Delta\gamma_{\text{eff}} = G$  (where  $G$  is the energy release rate). Note that only in this case the pull-off force can be correctly estimated by using the adapted JKR theory, i.e.  $F_{\text{off}} = (F_{\text{JKR}})_{\text{eff}} = 3\pi\Delta\gamma_{\text{eff}}R/2$ . Fig. 4 also reports the effect of the initial contact penetration  $\tilde{\Delta}_B$  on the normalized fast retraction pull-off force  $F_{\text{off}}/F_{\text{JKR}}$  and shows that the maximum pull-off enhancement reaches a plateau at high penetration (i.e., high preload), with  $F_{\text{off}}/F_{\text{JKR}} \approx E_\infty/E_0$  at very high retraction speed. Reducing the speed leads to smaller values of  $F_{\text{off}}/F_{\text{JKR}}$ , in agreement with [71].

In Fig.5 we report the effect on the adhesive contact behavior of the dimensionless dwell time  $\tilde{t}_d$ , i.e. the time delay between the end of the approaching stage and the initiation of the retraction process. Since the value  $\tilde{t}_d$  physically alters the stress-strain history, it necessarily affects the system response during retraction, while the approach stage is unaffected. We present results for dimensionless speed  $\tilde{V} = 0.1$ , and show that increasing  $\tilde{t}_d$  above 1 yields larger pull-off forces. To understand this peculiar behavior, we observe that the material relaxation increases with  $\tilde{t}_d$  and, for  $\tilde{t}_d \gg 1$ , the retraction behavior approaches the flat punch with very large pull off forces, as discussed above. Moreover, the A-R speed  $\tilde{V}$  plays a central role, as the increasing  $\tilde{V}$  require larger  $\tilde{t}_d$  values to achieve relaxation and, in turn, enter the flat-punch regime.

Figs. 6 reports the retraction behavior under load-controlled conditions assuming the same fully relaxed initial conditions (point B in the figure) as in Figs. 4. This time the tensile force is instantaneously applied following a step change to the negative value  $F_0 < -F_{\text{JKR}}$ , i.e.  $F(t) = F_B + (F_0 - F_B)H(t)$ . The application of this step change in the applied load leads to an initial high frequency glassy response of the system with modulus  $E_\infty$  so that the linear flat punch behavior is again recovered at the initial stages of the load controlled retraction.

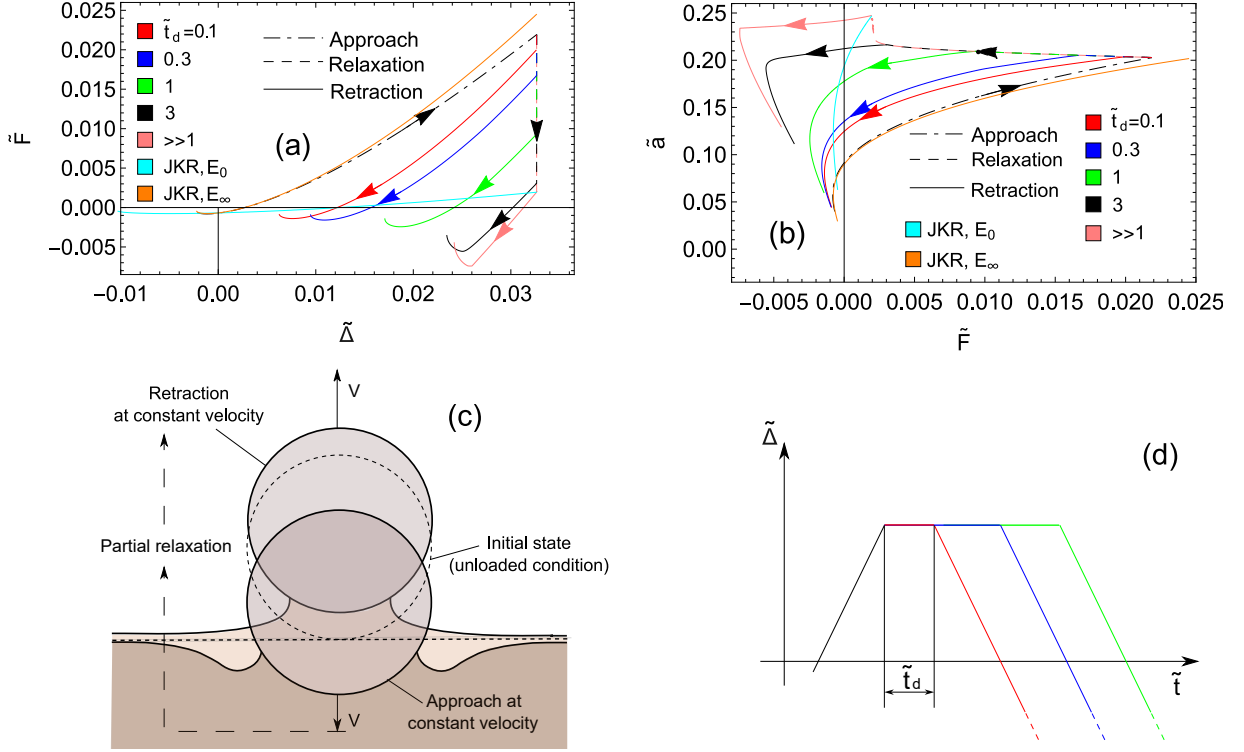


FIG. 5: Approach-retraction cycles with non-vanishing dimensionless dwell time  $\tilde{t}_d$ , allowing for partial material relaxation. The dimensionless sphere speed is  $\tilde{V} = 0.1$ . (a) The  $\tilde{F}$  vs.  $\tilde{\Delta}$  and (b) the  $\tilde{a}$  vs.  $\tilde{F}$  equilibrium diagrams for different values of  $\tilde{t}_d$ . (c) and (d) are the process schematic and the qualitative dimensionless penetration  $\tilde{\Delta}$  time-history, respectively. Results are shown for  $\tilde{\gamma} = 1.6 \times 10^{-4}$ ,  $E_\infty/E_0 = 10$ .

Then, the penetration also jumps to  $\Delta_0$  following the relation  $F_0 = F_B - 2a_B E_\infty^* (\Delta_B - \Delta_0)$ . After this step change, the contact area and the penetration  $\Delta$  monotonically decrease with time, as well as the retraction speed, and eventually becomes unstable and detach [see Fig. 6(b)]. This happens at significantly larger elongations (i.e., larger contact toughness) compared to  $V$ -controlled (dashed) curves associated with the same pull-off forces  $F_0$ .

Fig. 7 reports the contact behavior of the contact when the penetration oscillates and refers to  $\tilde{\gamma} = 5 \times 10^{-8}$  and  $\delta\tilde{a} = 8.5 \times 10^{-4}$ . Specifically, Fig. 7(a,b,c) presents results for a linear frequency sweep, i.e.  $\tilde{\Delta}(\tilde{t}) = \tilde{\Delta}_0 + \tilde{\Delta}_1 \sin[\tilde{\omega}(\tilde{t})\tilde{t}/2]$ , with  $\tilde{\omega} = \tau(d\theta/dt) = \alpha\tilde{t}$ ,  $\alpha = 0.006$ ,  $\tilde{\Delta}_1 = -1.7 \times 10^{-5}$ . The initial penetration  $\tilde{\Delta}_0 = 5.7 \times 10^{-5}$  corresponds to the fully-relaxed (modulus  $E_0$ ) JKR solution for  $\tilde{F} = 0$ . As the frequency is increased [see Fig.7(a,b)] the slope of the  $F$  vs.  $\Delta$  curve increases because of the material stiffening, see also [68, 72]. The amount of energy dissipated per cycle  $\tilde{L} = (1 - \nu^2)L/(\pi E_0 R^3)$  roughly equates the area of the cycle in the  $\Delta$  vs.  $\tilde{F}$  diagram and is reported in Fig. 7(c) as a function of the external excitation frequency  $\tilde{\omega}$ . The observed bell-shaped behavior is expected, as at very low and very high excitation frequencies the material behaves elastically, with vanishing hysteresis. At intermediate frequency (i.e.,  $\tilde{\omega} \approx 1$ ) the material response is in the transition region of the viscoelastic spectrum, and the viscoelastic energy dissipation takes its maximum value. More interestingly, Fig. 7(d) refers to the case of constant frequency oscillations (at different frequencies) superimposed to steady retraction at speed  $\tilde{V} = 10^{-7}$ , so that

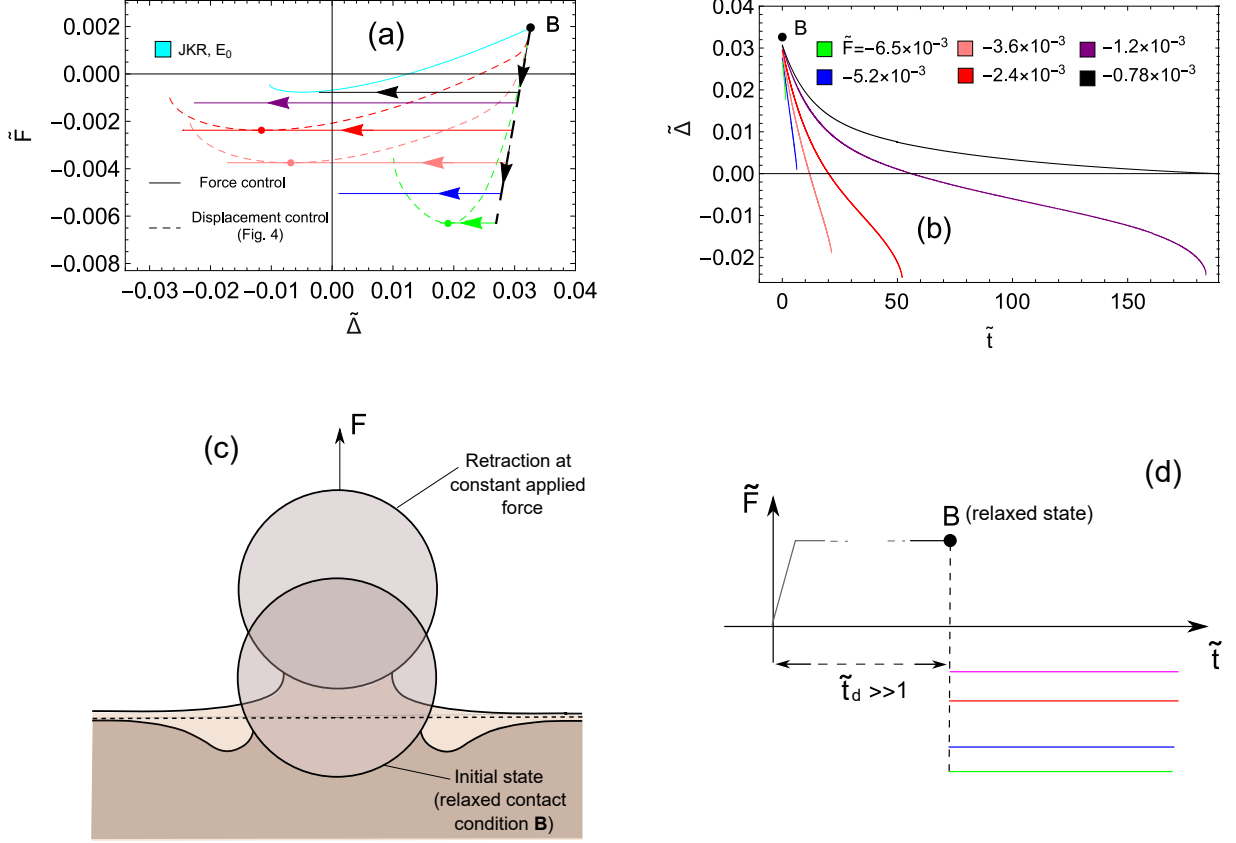


FIG. 6: The contact behavior under constant tensile force  $\tilde{F}$  instantaneously applied once the fully relaxed elastic condition is recovered (point B, with  $\tilde{\Delta}_B = 0.032$ ). (a) The  $\tilde{F}$  vs.  $\tilde{\Delta}$  equilibrium diagram for different values of the applied tensile force  $\tilde{F}$  (solid lines); in the same figure, the dashed line is the behavior at constant retraction velocity corresponding the same pull-off force. (b) The dimensionless indentation depth  $\tilde{\Delta}$  shown as function of the dimensionless time  $\tilde{t}$  for different values of the applied tensile force  $\tilde{F}$ . (c) and (d) are the process schematic and the qualitative dimensionless force  $\tilde{F}$  time-history, respectively. Results are shown for  $\tilde{\gamma} = 1.6 \times 10^{-4}$ ,  $E_\infty/E_0 = 10$ .

$\tilde{\Delta}(\tilde{t}) = \tilde{\Delta}_0 - \tilde{V}\tilde{t} + \tilde{\Delta}_2 \sin(\tilde{\omega}\tilde{t})$  with  $\tilde{\Delta}_2 = -8.5 \times 10^{-6}$ ,  $\tilde{\omega} = 0.35$  (orange line) and  $\tilde{\omega} = 1.4$  (blue line). Noteworthy, the envelopes of the maximum tensile loads (dashed lines) reached during the oscillating retraction stage significantly increase compared to the case of steady retraction (black curve, with no oscillations), thus paving the way to possible vibration based techniques to control interfacial adhesive strength, as experimentally observed by Shui *et al.* [23].

#### A. The energy release rate, the elastic energy, and viscoelastic energy dissipation.

In viscoelastic materials undergoing deformations, the work of internal stresses is partially stored as elastic potential energy and partially dissipated, leading to viscoelastic hysteresis.

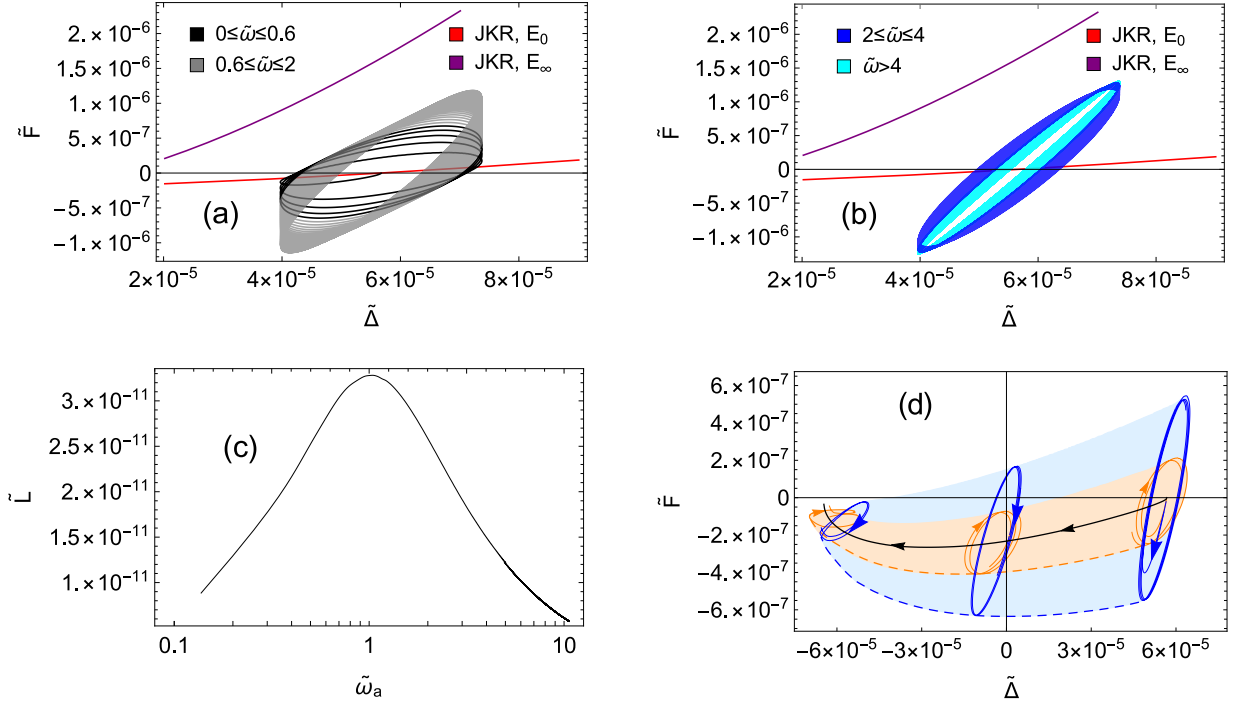


FIG. 7: Results for normal oscillations: (a,b,c) frequency (up-)sweep around a given dimensionless penetration  $\tilde{\Delta}_0$  with  $\tilde{\Delta}(\tilde{t}) = \tilde{\Delta}_0 + \tilde{\Delta}_1 \sin[\tilde{\omega}(\tilde{t})\tilde{t}/2]$  and  $\tilde{\omega}(\tilde{t}) = \alpha\tilde{t}$ ; (d) constant frequency oscillation superimposed to steady retraction at  $\tilde{V} = 10^{-7}$  from  $\tilde{\Delta}_0$  with  $\tilde{\Delta}(\tilde{t}) = \tilde{\Delta}_0 - \tilde{V}\tilde{t} + \tilde{\Delta}_2 \sin[\tilde{\omega}\tilde{t}]$ . Specifically, (a,b) are the equilibrium diagram for  $\tilde{F}$  vs.  $\tilde{\Delta}(t)$ , (c) is the dimensionless energy  $\tilde{L} = (1 - \nu^2)L/(\pi E_0 R^3)$  dissipated per cycle vs. the dimensionless frequency  $\tilde{\omega}_a$  averaged per cycle, and (d) are the equilibrium diagrams  $\tilde{F}$  vs.  $\tilde{\Delta}(t)$  for  $\tilde{\omega} = 0.35$  (orange line) and  $\tilde{\omega} = 1.4$  (blue line). Results refer to  $\tilde{\gamma} = 5 \times 10^{-8}$ ,  $E_\infty/E_0 = 10$ ,  $\tilde{\Delta}_0 = 5.7 \times 10^{-5}$ ,  $\tilde{\Delta}_1 = -1.7 \times 10^{-5}$ ,  $\tilde{\Delta}_2 = -8.5 \times 10^{-6}$ , and  $\alpha = 0.006$ .

Neglecting kinetic energy or inertia forces, energy balance requires the work per unit time of external and internal forces to be equal, i.e.

$$F \dot{\Delta} + \Delta \gamma \dot{A} = \dot{U} + P_d \quad (12)$$

where  $\dot{U}$  and  $P_d$  are the time-derivative of the stored elastic energy and the hysteretic energy losses per unit time, respectively. Most importantly, the energy release rate  $G$  can be defined also for non conservative materials [17, 37], as the change in the total mechanical energy per unit change in the contact area. Therefore, from Eq. (12), we have

$$G = \frac{\dot{U}}{\dot{A}} - F \frac{\dot{\Delta}}{\dot{A}} = \frac{dU}{dA} - F \frac{d\Delta}{dA}, \quad (13)$$

and

$$G = \Delta \gamma - P_d / \dot{A} \quad (14)$$

which shows that  $G$  is a key quantity in adhesive contact mechanics, sometimes referred to as the effective energy of adhesion or, in other words, the generalized driving force inducing the contact area change. Consequently, calculating  $G$  is a crucial (and usually tough) task, which requires to determine either  $\dot{U}$  or  $P_d$  as functions of the interfacial stress distribution  $\sigma(\mathbf{x}, t)$ .

Aiming at accomplishing this task, we calculate the work per unit time  $P$  done by the internal stresses which, at equilibrium is only related to the stress and displacement distributions on the half-space surface. In the most general case (i.e., neglecting axial symmetry), we have

$$\begin{aligned} P(t) &= \int d^2x \sigma(\mathbf{x}, t) \dot{u}(\mathbf{x}, t) \\ &= \int d^2x d^2x_1 \mathcal{G}(\mathbf{x} - \mathbf{x}_1) \sigma(\mathbf{x}, t) \dot{\varepsilon}(\mathbf{x}_1, t) \end{aligned} \quad (15)$$

where

$$\varepsilon(\mathbf{x}, t) = \int_{-\infty}^t dt_1 J(t - t_1) \dot{\sigma}(\mathbf{x}, t_1) = \varepsilon_0(\mathbf{x}, t) + \sum_{k=1}^n \varepsilon_k(\mathbf{x}, t) \quad (16)$$

is an apparent local surface strain,  $J(t) = E_\infty^{-1} + \sum_{k=1}^n E_k^{-1} [1 - \exp(-t/\tau_k)]$  is the creep function for a generic linear viscoelastic material with an arbitrary number  $n$  of relaxation times  $\tau_k$ , and

$$\begin{aligned} \varepsilon_0(\mathbf{x}, t) &= \frac{\sigma(\mathbf{x}, t)}{E_\infty} \\ \varepsilon_k(\mathbf{x}, t) &= \int_{-\infty}^t dt_1 \frac{1}{E_k} \left[ 1 - \exp\left(-\frac{t - t_1}{\tau_k}\right) \right] \dot{\sigma}(\mathbf{x}, t_1) \end{aligned} \quad (17)$$

are, respectively, the elastic contribution to  $\varepsilon$  associated with the high-frequency modulus  $E_\infty$ , and the viscoelastic contributions associated with each single  $k$ th Voigt element. We then have

$$\sigma(\mathbf{x}, t) = E_\infty \varepsilon_0(\mathbf{x}, t) = E_k \varepsilon_k(\mathbf{x}, t) + \tau_k E_k \dot{\varepsilon}_k(\mathbf{x}, t), \quad k = 1, \dots, n \quad (18)$$

where  $E_k \varepsilon_k(\mathbf{x}, t)$  and  $\tau_k E_k \dot{\varepsilon}_k(\mathbf{x}, t)$  represent, respectively, the elastic and viscous stress components associated with the  $k$ -th Voigt element. Combining Eqs. (15, 16, 17, 18) gives the expression of the elastic  $\dot{U}$  and dissipative  $P_d$  contributions to  $P$  (i.e.,  $P = \dot{U} + P_d$ ). In particular,

$$\dot{U}(t) = \int d^2x d^2x_1 \mathcal{G}(\mathbf{x} - \mathbf{x}_1) \left[ E_\infty \varepsilon_0(\mathbf{x}, t) \dot{\varepsilon}_0(\mathbf{x}_1, t) + \sum_{k=1}^n E_k \varepsilon_k(\mathbf{x}, t) \dot{\varepsilon}_k(\mathbf{x}_1, t) \right] \quad (19)$$

and

$$P_d(t) = \sum_{k=1}^n \int d^2x d^2x_1 \mathcal{G}(\mathbf{x} - \mathbf{x}_1) \tau_k E_k \dot{\varepsilon}_k(\mathbf{x}, t) \dot{\varepsilon}_k(\mathbf{x}_1, t) \quad (20)$$

Note that in Eq. (19) the quantity  $\mathcal{G}(\mathbf{x})$  is a symmetric function so that it is possible to find the expression of the elastic energy as

$$U(t) = \frac{1}{2} \int d^2x d^2x_1 \mathcal{G}(\mathbf{x} - \mathbf{x}_1) \left[ E_\infty \varepsilon_0(\mathbf{x}, t) \varepsilon_0(\mathbf{x}_1, t) + \sum_{k=1}^n E_k \varepsilon_k(\mathbf{x}, t) \varepsilon_k(\mathbf{x}_1, t) \right] \quad (21)$$

The energy release rate  $G$  can be calculated using Eqs. (13, 19) at any given time  $t$  once solved the elastic problem, i.e. for known values of  $\sigma(\mathbf{x}, t)$ ,  $u(\mathbf{x}, t)$ , and the contact domain  $\Omega(t)$ .

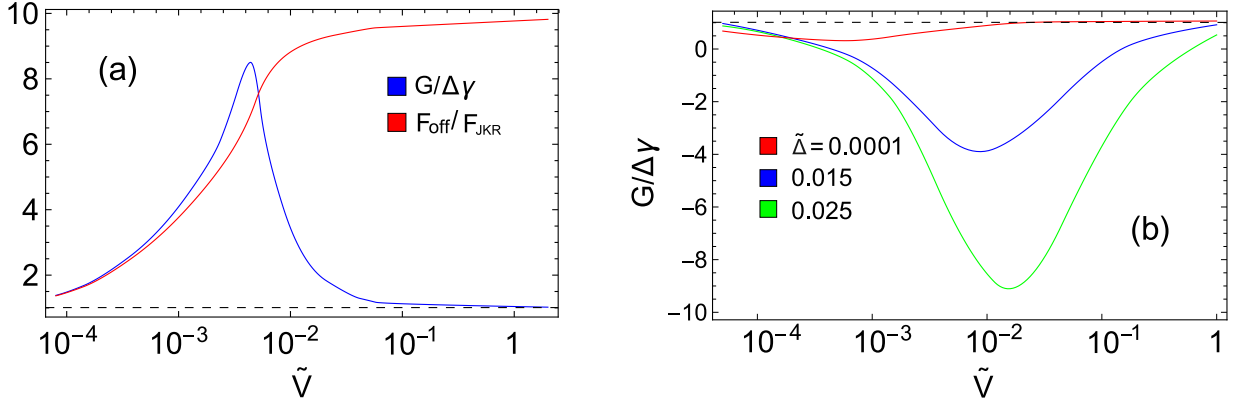


FIG. 8: The normalized energy release rate  $G/\Delta\gamma$  (a) at pull-off (blue line) and (b) during indentation (for different dimensionless penetrations  $\tilde{\Delta}$ ) as functions of the dimensionless velocity. The viscoelastic-elastic pull-off force ratio  $F_{\text{off}}/F_{\text{JKR}}$  is also shown in (a) as red line. Initial condition in (a) refers to fully relaxed state (point  $B$  in Fig. 4). Results are shown for  $\tilde{\gamma} = 1.6 \times 10^{-4}$ ,  $E_{\infty}/E_0 = 10$ .

Recalling that  $G = \Delta\gamma - P_d/\dot{A}$  and considering that  $P_d > 0$ , we find that during the approach stage (i.e.,  $\dot{A} > 0$ ) the energy release rate  $G < \Delta\gamma$  and can be even negative, whereas during retraction (i.e.,  $\dot{A} < 0$ ) the energy release rate  $G > \Delta\gamma$ . Figure 8 reports the trends of the normalized energy release rate  $G/\Delta\gamma$  vs. speed, during (a) retraction and (b) approach stages. More specifically,  $P_d$  vanishes at very-low and very-large A-R speeds, so that in these two limiting cases  $G(t) \rightarrow \Delta\gamma$ . At intermediate speed it increases up to a maximum value, with the resulting bell-shaped behavior being related to the presence of a reference length scale (i.e., finite contact size) [17, 37, 62, 63]. For comparison, we stress that the propagation of a opening semi-infinite crack in an infinite systems represents a very different scenario, as in this case  $P_d$  must monotonically increase with crack speed and eventually reach a plateau (for isothermal conditions) [43, 64–66, 83]. Noteworthy, since  $P_d$  accounts for the energy dissipation in the whole viscoelastic material, it can also take values such that  $P_d/\dot{A} > \Delta\gamma$ , thus entailing  $G(t) < 0$  when the sphere is pressed against the viscoelastic half-space [see Fig. 8(b)]. Fig. 8(a) also reports the normalized maximum tensile load (i.e. the pull-off force) as a function of the retraction speed. It is very important to notice that, despite the bell-shaped rate  $G(t)$  vs.  $\tilde{V}$  trend, the ratio  $F_{\text{off}}/F_{\text{JKR}}$  continuously increases until a limiting value is reached ( $F_{\text{off}}/F_{\text{JKR}} \approx E_{\infty}/E_0$ ). A deeper look at the retraction behavior [Fig. 8(a)] also shows that  $G/\Delta\gamma \approx F_{\text{off}}/F_{\text{JKR}}$  only at relatively low retraction speeds, i.e. for  $\tilde{V} \lesssim 5 \times 10^{-4}$ . This is the limit where small-scale viscoelasticity (i.e., localized non-conservative phenomena close to the edge of the contact) governs the adhesion enhancement [17, 37, 67], and JKR pull-off approximation  $F_{\text{off}} = (F_{\text{JKR}})_{\text{eff}} = 3\pi\Delta\gamma_{\text{eff}}R/2$  holds true (allowing for a rough estimation of  $G = \Delta\gamma_{\text{eff}}$ ). Differently, at large retraction speeds, both the small- and large-scale viscoelasticity vanish (e.g.,  $G \rightarrow \Delta\gamma$ ), and the pull-off is governed by the glassy flat punch behavior, as discussed in Sec. III. To the best of authors knowledge, this is a novel finding, as previous numerical studies on viscoelastic adhesive contacts (with gap-dependent adhesion) [31, 68, 71, 77] relied on JKR pull-off equation to estimate the energy release rate  $G$  even at high retraction speed.

## IV. CONCLUSIONS

We study the problem of the unsteady normal indentation of a rigid sphere into a viscoelastic half-space, in the presence of interfacial adhesion. To solve the problem, we developed a novel energy-based approach, which generalizes the Griffith fracture criterion also to time-dependent unsteady non-conservative contacts. We also present a rigorous procedure to accurately calculate the time evolution of the elastic energy, the viscoelastic energy dissipation, and energy release rate  $G$ , by relying only on the interfacial stress and displacement distributions. We predict that, depending on the specific time-history of the contact process, the effective adhesion may be significantly enhanced by viscoelasticity. At intermediate approach-retraction speeds, strong adhesive hysteresis is observed because of small-scale viscoelastic dissipation localized close to the perimeter of the contact area, which also entails the ability of the system to withstand very high tensile loads. Hysteresis vanishes at very high and very low approach-retraction speed as the material response falls, respectively, in the high frequency (stiff) or low frequency (soft) elastic regimes. More importantly, our theory predicts the extremely large pull-off forces observed experimentally when retraction starts from a completely relaxed loaded state, with sufficiently high retraction speed. In this case, the material has no time to relax and exhibits a ‘frozen’ glassy elastic state, thus resembling the behavior of a flat-punch with a linear force-penetration relation. We also show that at sufficiently large retraction speed  $V$ , the energy release rate reduces with the increasing  $V$  down to the thermodynamic surface energy value  $\Delta\gamma$ . However, in such conditions the contact behavior significantly deviates from JKR theory as small-scale viscoelasticity cannot be invoked in this case. This implies that the JKR model cannot be employed to estimate the energy release from pull-off force at high retraction speeds, as this procedure significantly overestimates  $G$ .

### Acknowledgments

This work was partly supported by the Italian Ministry of University and Research under the Programme “Department of Excellence ” (decree 232/2016) and partly by the European Union - NextGenerationEU through the Italian Ministry of University and Research under the programs: (GC) National Sustainable Mobility Center CN00000023 (decree nr. 1033 - 17/06/2022), Spoke 11 – Innovative Materials Lightweighting; (NM) PRIN2022 (grant nr. 2022SJ8HTC) and PRIN2022 PNRR (grant nr. P2022MAZHX). The opinions expressed are those of the authors only and should not be considered as representative of the European Union or the European Commission’s official position. Neither the European Union nor the European Commission can be held responsible for them.

### Appendix A: Numerical implementation

In this section, we outline the numerical procedure to solve Eq. (1). We refer to the viscoelastic creep’s function with single relaxation time given by Eq. (11). In this case,

taking the time derivative of Eq. (1) leads to

$$\dot{u}(\mathbf{x}, t) = \frac{1}{E_\infty} \int dx_1^2 \mathcal{G}(\mathbf{x} - \mathbf{x}_1) \dot{\sigma}(\mathbf{x}_1, t) \quad (\text{A1})$$

$$\begin{aligned} & - \frac{1}{\tau^2 E_1} \exp\left(-\frac{t}{\tau}\right) \int_{-\infty}^t dt_1 \exp\left(\frac{t_1}{\tau}\right) \int dx_1^2 \mathcal{G}(\mathbf{x} - \mathbf{x}_1) \sigma(\mathbf{x}_1, t_1) \quad (\text{A2}) \\ & + \frac{1}{\tau E_1} \int dx_1^2 \mathcal{G}(\mathbf{x} - \mathbf{x}_1) \sigma(\mathbf{x}_1, t) \end{aligned}$$

Using again Eqs. (1, 11) yields the following time-differential equation:

$$\dot{u}(\mathbf{x}, t) = \frac{1}{E_\infty} \int dx_1^2 \mathcal{G}(\mathbf{x} - \mathbf{x}_1) \dot{\sigma}(\mathbf{x}_1, t) + \frac{1}{\tau E_0} \int dx_1^2 \mathcal{G}(\mathbf{x} - \mathbf{x}_1) \sigma(\mathbf{x}_1, t) - \frac{u(\mathbf{x}, t)}{\tau} \quad (\text{A3})$$

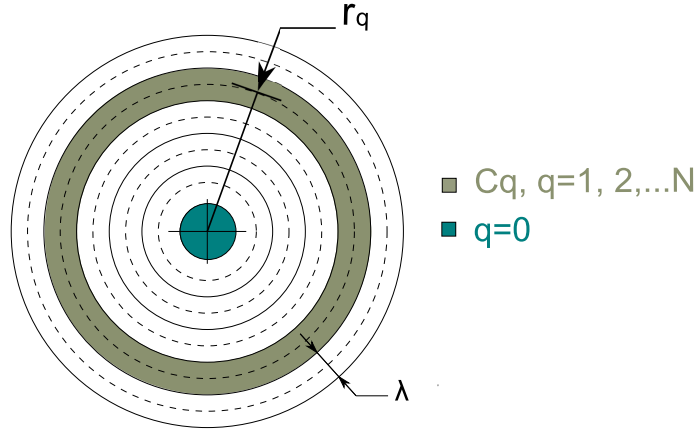


FIG. 9: The discretization of spatial domain for the numerical resolution of Eq. 1

which can be solved avoiding integration over the whole time history. Using a numerical quadrature rule and exploiting the axisymmetric nature of the problem, the spatial domain is discretized as shown in Fig. 9 into  $N$  circular annulus  $C_q$  of constant width  $\lambda$  (with  $\lambda/a \ll 1$ ) placed at radii  $r_q = q\lambda + \lambda/2$ , and a circle  $C_0$  of radius  $\lambda$  placed at  $r_0 = 0$ . Each area is subjected to uniform stress  $\sigma_q(t) = \sigma(r_q, t)$ ,  $q = 0, 1, \dots, N$ , and Eq.A3 can be rewritten as

$$\dot{u}_h(t) = \dot{u}(r_h, t) = \frac{1}{E_\infty} \sum_{q=0}^N \dot{\sigma}_q(t) \int_{C_q} dx_1^2 \mathcal{G}(\mathbf{x} - \mathbf{x}_1) + \frac{1}{\tau E_0} \sum_{q=0}^N \sigma_q(t) \int_{C_q} dx_1^2 \mathcal{G}(\mathbf{x} - \mathbf{x}_1) - \frac{u_h(t)}{\tau} \quad (\text{A4})$$

where  $\int_{C_q} dx_1^2 \mathcal{G}(\mathbf{x} - \mathbf{x}_1) = \tilde{\mathcal{G}}(r_h, r_q) = \tilde{\mathcal{G}}_{hq}$  is an axisymmetric field that represents the surface displacement at radius  $r_h$  induced on an elastic half-space of unit modulus by a uniform unit stress acting over  $C_q$ .  $\tilde{\mathcal{G}}_{hq}$  can be easily calculated. Indeed, following [57, 81], the quantity

$$\mathcal{K}(r_h, r_q) = \begin{cases} (1 - \nu^2) \pi^{-1} 4r_q \mathbf{E}(r_h/r_q), & r_h \leq r_q \\ (1 - \nu^2) \pi^{-1} 4r_h [\mathbf{E}(r_q/r_h) - (1 - (r_q/r_h)^2) \mathbf{K}(r_q/r_h)], & r_h > r_q \end{cases} \quad (\text{A5})$$

is the surface displacement at radius  $r_h$  resulting from a uniform unit stress field acting over a circle of radius  $r_q$  in the elastic problem (notably, a similar solution is given in Ref. [82] for uniform tangential stresses). In Eq. (A5),  $\mathbf{K}(\rho) = \int_0^{\pi/2} d\xi (1 - \rho^2 \sin^2(\xi))^{-1/2}$  and  $\mathbf{E}(\rho) = \int_0^{\pi/2} d\xi (1 - \rho^2 \sin^2(\xi))^{1/2}$  are the complete elliptic integrals of the first and second kind, respectively. Thus, according to Fig. 9,  $\tilde{\mathcal{G}}_{h0} = \mathcal{K}(r_h, \lambda)$  and, using the superposition of effects:

$$\tilde{\mathcal{G}}_{hq} = \mathcal{K}(r_h, r_q + \lambda/2) - \mathcal{K}(r_h, r_q - \lambda/2), \quad q \neq 0 \quad (\text{A6})$$

The time domain is discretized with small steps  $\varepsilon$ , with  $\varepsilon/\tau \ll 1$  and the discrete form of Eq. A3 can be written at time  $t_k = k\varepsilon$  with  $k = 1, 2, \dots$ . Note that we define  $u_h^k(r_h, t_k)$  and  $\sigma_h^k = \sigma(r_h, t_k)$  and write

$$\left(1 + \frac{\varepsilon}{\tau}\right) u_h^k = \left(\frac{1}{E_\infty} + \frac{\varepsilon}{\tau E_0}\right) \sum_{q=0}^N \tilde{\mathcal{G}}_{hq} \sigma_q^k + A_h^{k-1} \quad (\text{A7})$$

where the quantity

$$A_h^k = u_h^k - \frac{1}{E_\infty} \sum_{q=0}^N \tilde{\mathcal{G}}_{hq} \sigma_q^k \quad (\text{A8})$$

has already been determined up to time  $t^{k-1}$ . The linear system of equations Eq. (A7)

allows to calculate, for any given value of the contact radius  $a$ , the stress distribution in the contact area and the displacement and gap distributions out of the contact area. Then, enforcing the energy balance condition Eq. (9) the equilibrium value  $a^k = a(t^k)$  of the contact radius can be determined.

- 
- [1] Johnson, K. L., Kendall, K., Roberts, A. (1971). Surface energy and the contact of elastic solids. Proceedings of the royal society of London. A. mathematical and physical sciences, 324(1558), 301-313
  - [2] Griffith, A. A. (1921). VI. The phenomena of rupture and flow in solids. Philosophical transactions of the royal society of london. Series A, containing papers of a mathematical or physical character, 221(582-593), 163-198.
  - [3] Das, S., Lahiri, D., Lee, D. Y., Agarwal, A., & Choi, W. (2013). Measurements of the adhesion energy of graphene to metallic substrates. Carbon, 59, 121-129.
  - [4] Gruhn, T., Franke, T., Dimova, R., & Lipowsky, R. (2007). Novel method for measuring the adhesion energy of vesicles. Langmuir, 23(10), 5423-5429.
  - [5] Raegen, A. N., Dalnoki-Veress, K., Wan, K. T., & Jones, R. A. L. (2006). Measurement of adhesion energies and Young's modulus in thin polymer films using a novel axi-symmetric peel test geometry. The European Physical Journal E, 19, 453-459.
  - [6] Maugis, D. (1992). Adhesion of spheres: the JKR-DMT transition using a Dugdale model. Journal of colloid and interface science, 150(1), 243-269.
  - [7] Guduru, P. R. (2007). Detachment of a rigid solid from an elastic wavy surface: theory. Journal of the Mechanics and Physics of Solids, 55(3), 445-472.

- [8] Greenwood, J. A., & Williamson, J. B. P., 1966. Contact of Nominally Flat Surfaces. *Proceedings of the Royal Society A: Mathematical, Physical and Engineering Sciences*, 295(1442), 300–319.
- [9] Carbone, G., Scaraggi, M., & Tartaglino, U. (2009). Adhesive contact of rough surfaces: comparison between numerical calculations and analytical theories. *The European Physical Journal E*, 30, 65-74.
- [10] Carbone, G., Mangialardi, L., & Persson, B. N. J. (2004). Adhesion between a thin elastic plate and a hard randomly rough substrate. *Physical Review B*, 70(12), 125407.
- [11] Menga, N., Carbone, G., & Dini, D. (2018). Do uniform tangential interfacial stresses enhance adhesion?. *Journal of the Mechanics and Physics of Solids*, 112, 145-156.
- [12] Menga, N., Carbone, G., & Dini, D. (2019). Corrigendum to “Do uniform tangential interfacial stresses enhance adhesion?” [*Journal of the Mechanics and Physics of Solids* 112 (2018) 145–156].
- [13] Lin, Y. Y., Chang, C. F., & Lee, W. T. (2008). Effects of thickness on the largely-deformed JKR (Johnson–Kendall–Roberts) test of soft elastic layers. *International Journal of Solids and Structures*, 45(7-8), 2220-2232.
- [14] Carbone, G., & Mangialardi, L. (2008). Analysis of the adhesive contact of confined layers by using a Green’s function approach. *Journal of the Mechanics and Physics of Solids*, 56(2), 684-706.
- [15] Carbone, G., Pierro, E., & Gorb, S. N. (2011). Origin of the superior adhesive performance of mushroom-shaped microstructured surfaces. *Soft Matter*, 7(12), 5545-5552.
- [16] Menga, N., Afferrante, L., & Carbone, G. (2016). Adhesive and adhesiveless contact mechanics of elastic layers on slightly wavy rigid substrates. *International Journal of Solids and Structures*, 88, 101-109.
- [17] Carbone, G., Mandriota, C., & Menga, N. (2022). Theory of viscoelastic adhesion and friction. *Extreme Mechanics Letters*, 56, 101877.
- [18] Charrault, E., Gauthier, C., Marie, P., & Schirrer, R. (2009). Experimental and theoretical analysis of a dynamic JKR contact. *Langmuir*, 25(10), 5847-5854.
- [19] Linghu, C., Yang, X., Liu, Y., Li, D., Gao, H., & Hsia, K. J. (2023). Mechanics of shape-locking-governed R2G adhesion with shape memory polymers. *Journal of the Mechanics and Physics of Solids*, 170, 105091.
- [20] Violano, G., & Afferrante, L. (2019). Adhesion of compliant spheres: An experimental investigation. *Procedia Structural Integrity*, 24, 251-258.
- [21] Ahn, D., & Shull, K. R. (1996). JKR studies of acrylic elastomer adhesion to glassy polymer substrates. *Macromolecules*, 29(12), 4381-4390.
- [22] Li, M., Jiao, Q., Dai, Q., Shi, L., Huang, W., & Wang, X. (2019). Effects of bulk viscoelasticity and surface wetting on the contact and adhesive properties of a soft material. *Polymer Testing*, 74, 266-273.
- [23] Shui, L., Jia, L., Li, H., Guo, J., Guo, Z., Liu, Y., ... & Chen, X. (2020). Rapid and continuous regulating adhesion strength by mechanical micro-vibration. *Nature communications*, 11(1), 1583.
- [24] Lin, Y. Y., & Hui, C. Y. (2002). Mechanics of contact and adhesion between viscoelastic spheres: an analysis of hysteresis during loading and unloading. *Journal of Polymer Science Part B: Polymer Physics*, 40(9), 772-793.
- [25] Greenwood, J. A., & Johnson, K. L. (2006). Oscillatory loading of a viscoelastic adhesive contact. *Journal of colloid and interface science*, 296(1), 284-291.

- [26] Giri, M., Bousfield, D. B., & Unertl, W. N. (2001). Dynamic contacts on viscoelastic films: work of adhesion. *Langmuir*, 17(10), 2973-2981.
- [27] Luo, J., Liu, J., Xia, H., Ao, X., Fu, Z., Ni, J., & Huang, H. (2024). Finite Element Analysis of Adhesive Contact Behaviors in Elastoplastic and Viscoelastic Media. *Tribology Letters*, 72(1), 7.
- [28] Afferrante, L., Violano, G., & Carbone, G. (2023). Exploring the dynamics of viscoelastic adhesion in rough line contacts. *Scientific Reports*, 13(1), 15060.
- [29] Haiat, G., Huy, M. P., & Barthel, E. (2003). The adhesive contact of viscoelastic spheres. *Journal of the Mechanics and Physics of Solids*, 51(1), 69-99.
- [30] Baek, D., Hemthavy, P., Saito, S., & Takahashi, K. (2017). Evaluation of energy dissipation involving adhesion hysteresis in spherical contact between a glass lens and a PDMS block. *Applied Adhesion Science*, 5, 1-11.
- [31] Müser, M. H., & Persson, B. N. (2022). Crack and pull-off dynamics of adhesive, viscoelastic solids. *Europhysics Letters*, 137(3), 36004.
- [32] Müser, M. H., Sukhomlinov, S. V., & Pastewka, L. (2023). Interatomic potentials: Achievements and challenges. *Advances in Physics: X*, 8(1), 2093129.
- [33] Lorenz, B., Krick, B. A., Mulakaluri, N., Smolyakova, M., Dieluweit, S., Sawyer, W. G., & Persson, B. N. J. (2013). Adhesion: role of bulk viscoelasticity and surface roughness. *Journal of Physics: Condensed Matter*, 25(22), 225004.
- [34] Das, D., & Chasiotis, I. (2021). Rate dependent adhesion of nanoscale polymer contacts. *Journal of the Mechanics and Physics of Solids*, 156, 104597.
- [35] Jiang, L., Wu, M., Yu, Q., Shan, Y., & Zhang, Y. (2021). Investigations on the adhesive contact behaviors between a viscoelastic stamp and a transferred element in microtransfer printing. *Coatings*, 11(10), 1201.
- [36] Johnson, K. L. (2000). Contact mechanics and adhesion of viscoelastic spheres.
- [37] Mandriota, C., Menga, N., & Carbone, G. (2024). Adhesive contact mechanics of viscoelastic materials. *International Journal of Solids and Structures*, 112685.
- [38] Carbone, G., & Putignano, C. (2013). A novel methodology to predict sliding and rolling friction of viscoelastic materials: Theory and experiments. *Journal of the Mechanics and Physics of Solids*, 61(8), 1822-1834.
- [39] Putignano, C., & Carbone, G. (2022). Indenting viscoelastic thin layers: A numerical assessment. *Mechanics Research Communications*, 126, 104011.
- [40] Haiat, G., & Barthel, E. (2007). An approximate model for the adhesive contact of rough viscoelastic surfaces. *Langmuir*, 23(23), 11643-11650.
- [41] Kendall, K. (1971). The adhesion and surface energy of elastic solids. *Journal of Physics D: Applied Physics*, 4(8), 1186.
- [42] Schapery, R. A. (1975). A theory of crack initiation and growth in viscoelastic media: I. Theoretical development. *International Journal of fracture*, 11, 141-159.
- [43] Schapery, R. A. (1989). On the mechanics of crack closing and bonding in linear viscoelastic media. *International Journal of Fracture*, 39, 163-189.
- [44] Bitner, J. L., Rushford, J. L., Rose, W. S., Hunston, D. L., & Riew, C. K. (1981). Viscoelastic fracture of structural adhesives. *The Journal of Adhesion*, 13(1), 3-28.
- [45] Sancaktar, E., & Brinson, H. F. (1980). The viscoelastic shear behavior of a structural adhesive. In *Adhesion and Adsorption of Polymers* (pp. 279-299). Boston, MA: Springer US.
- [46] Chang, E. P. (1997). Viscoelastic properties of pressure-sensitive adhesives. *The Journal of Adhesion*, 60(1-4), 233-248.

- [47] Montazeri, S., Ranjbar, Z., & Rastegar, S. (2017). A study on effects of viscoelastic properties on protective performance of epoxy coatings using EIS. *Progress in Organic Coatings*, 111, 248-257.
- [48] Favi, P. M., Yi, S., Lenaghan, S. C., Xia, L., & Zhang, M. (2014). Inspiration from the natural world: from bio-adhesives to bio-inspired adhesives. *Journal of Adhesion Science and Technology*, 28(3-4), 290-319.
- [49] Purto, J., Frensemeier, M., & Kroner, E. (2015). Switchable adhesion in vacuum using bio-inspired dry adhesives. *ACS applied materials & interfaces*, 7(43), 24127-24135.
- [50] Zaokari, Y., Persaud, A., & Ibrahim, A. (2020). Biomaterials for adhesion in orthopedic applications: a review. *Engineered Regeneration*, 1, 51-63.
- [51] Shah, N. V., & Meislin, R. (2013). Current state and use of biological adhesives in orthopedic surgery. *Orthopedics*, 36(12), 945-956.
- [52] Stan, G., & Adams, G. G. (2016). Adhesive contact between a rigid spherical indenter and an elastic multi-layer coated substrate. *International journal of solids and structures*, 87, 1-10.
- [53] Ding, J. N., Meng, Y. G., & Wen, S. Z. (2000). Mechanical Stability and Sticking in a Model Microelectromechanical Systems (MEMS) under Casimir Forces—Part I: Corrections to the Casimir Force. *International Journal of Nonlinear Sciences and Numerical Simulation*, 1(Supplement), 373-378.
- [54] Taran, B., Amoozegar, S., Bayaz, R. N. D., & Barazandeh, F. (2011, May). The theoretical investigation of the effect of adhesive layers used in microassembly on the dynamic response of a microaccelerometer. In *2011 Symposium on Design, Test, Integration & Packaging of MEMS/MOEMS (DTIP)* (pp. 1-6). IEEE.
- [55] Cecil\*, J., Vasquez, D., & Powell, D. (2005). A review of gripping and manipulation techniques for micro-assembly applications. *International Journal of Production Research*, 43(4), 819-828.
- [56] Alogla, A. F., Amalou, F., Balmer, C., Scanlan, P., Shu, W., & Reuben, R. L. (2015). Micro-tweezers: Design, fabrication, simulation and testing of a pneumatically actuated micro-gripper for micromanipulation and microtactile sensing. *Sensors and Actuators A: Physical*, 236, 394-404.
- [57] Johnson, K. L., & Johnson, K. L. (1987). *Contact mechanics*. Cambridge university press.
- [58] Schapery, R. A. (1964). On the time dependence of viscoelastic variational solutions. *Quarterly of Applied Mathematics*, 22(3), 207-215.
- [59] Biot, M. (1955). Variational principles in irreversible thermodynamics with application to viscoelasticity. *Physical Review*, 97(6), 1463.
- [60] Gurtin, M. E. (1963). Variational principles in the linear theory of viscoelasticity. *Archive for Rational Mechanics and Analysis*, 13, 179-191.
- [61] de Gennes, P. G. (1996). Soft adhesives. *Langmuir*, 12(19), 4497-4500.
- [62] Persson, B. N. J. (2017). Crack propagation in finite-sized viscoelastic solids with application to adhesion. *Europhysics Letters*, 119(1), 18002.
- [63] Persson, B. N. J. (2021). On opening crack propagation in viscoelastic solids. *Tribology Letters*, 69(3), 115.
- [64] Persson, B. N. J., & Brener, E. A. (2005). Crack propagation in viscoelastic solids. *Physical Review E*, 71(3), 036123.
- [65] Greenwood, J. A. (2004). The theory of viscoelastic crack propagation and healing. *Journal of Physics D: Applied Physics*, 37(18), 2557.
- [66] Barber, M., Donley, J., & Langer, J. S. (1989). Steady-state propagation of a crack in a viscoelastic strip. *Physical Review A*, 40(1), 366.

- [67] Carbone, G., & Mangialardi, L. (2004). Adhesion and friction of an elastic half-space in contact with a slightly wavy rigid surface. *Journal of the Mechanics and Physics of Solids*, 52(6), 1267-1287.
- [68] Afferrante, L., & Violano, G. (2022). On the effective surface energy in viscoelastic Hertzian contacts. *Journal of the Mechanics and Physics of Solids*, 158, 104669.
- [69] Persson, B. N., & Scaraggi, M. (2014). Theory of adhesion: Role of surface roughness. *The Journal of chemical physics*, 141(12).
- [70] Greenwood, J. A. (2007). Viscoelastic crack propagation and closing with Lennard-Jones surface forces. *Journal of Physics D: Applied Physics*, 40(6), 1769.
- [71] Violano, G., & Afferrante, L. (2022). Size effects in adhesive contacts of viscoelastic media. *European Journal of Mechanics-A/Solids*, 96, 104665.
- [72] Menga, N., Afferrante, L., & Carbone, G. (2016). Effect of thickness and boundary conditions on the behavior of viscoelastic layers in sliding contact with wavy profiles. *Journal of the Mechanics and Physics of Solids*, 95, 517-529
- [73] Menga, N., Putignano, C., Afferrante, L., & Carbone, G. (2019). The contact mechanics of coated elastic solids: Effect of coating thickness and stiffness. *Tribology Letters*, 67, 1-10.
- [74] Akulich, A. G., Tiwari, A., Dorogin, L., Echtermeyer, A. T., & Persson, B. N. J. (2018). Rubber adhesion below the glass transition temperature: Role of frozen-in elastic deformation. *Europhysics Letters*, 120(3), 36002.
- [75] Menga, N., Putignano, C., Carbone, G., & Demelio, G. P. (2014). The sliding contact of a rigid wavy surface with a viscoelastic half-space. *Proceedings of the Royal Society A: Mathematical, Physical and Engineering Sciences*, 470(2169), 20140392.
- [76] Deruelle, M., Hervet, H., Jandeau, G., & Léger, L. (1998). Some remarks on JKR experiments. *Journal of adhesion science and technology*, 12(2), 225-247.
- [77] Lin, Y. Y., & Hui, C. Y. (2002). Mechanics of contact and adhesion between viscoelastic spheres: an analysis of hysteresis during loading and unloading. *Journal of Polymer Science Part B: Polymer Physics*, 40(9), 772-793.
- [78] Pérez-Ràfols, F., Van Dokkum, J. S., & Nicola, L. (2023). On the interplay between roughness and viscoelasticity in adhesive hysteresis. *Journal of the Mechanics and Physics of Solids*, 170, 105079.
- [79] Shull, K. R. (2002). Contact mechanics and the adhesion of soft solids. *Materials Science and Engineering: R: Reports*, 36(1), 1-45.
- [80] Hui, C. Y., Liu, T., Salez, T., Raphael, E., & Jagota, A. (2015). Indentation of a rigid sphere into an elastic substrate with surface tension and adhesion. *Proceedings of the Royal Society A: Mathematical, Physical and Engineering Sciences*, 471(2175), 20140727.
- [81] Lubarda, V. A. (2013). Circular loads on the surface of a half-space: displacement and stress discontinuities under the load. *International Journal of Solids and Structures*, 50(1), 1-14.
- [82] Menga, N., & Carbone, G. (2019). The surface displacements of an elastic half-space subjected to uniform tangential tractions applied on a circular area. *European Journal of Mechanics-A/Solids*, 73, 137-143.
- [83] Carbone, G., & Persson, B. N. J. (2005). Hot cracks in rubber: origin of the giant toughness of rubberlike materials. *Physical review letters*, 95(11), 114301.
- [84] Menga, N., Dini, D., & Carbone, G. (2020). Tuning the periodic V-peeling behavior of elastic tapes applied to thin compliant substrates. *International Journal of Mechanical Sciences*, 170, 105331.
- [85] Menga, N., Afferrante, L., Pugno, N. M., & Carbone, G. (2018). The multiple V-shaped double

- peeling of elastic thin films from elastic soft substrates. *Journal of the Mechanics and Physics of Solids*, 113, 56-64.
- [86] Charmet, J. C., & Barquins, M. (1996). Adhesive contact and rolling of a rigid cylinder under the pull of gravity on the underside of a smooth-surfaced sheet of rubber. *International journal of adhesion and adhesives*, 16(4), 249-254.
- [87] Davis, C. S., Lemoine, F., Darnige, T., Martina, D., Creton, C., & Lindner, A. (2014). Debonding mechanisms of soft materials at short contact times. *Langmuir*, 30(35), 10626-10636
- [88] Luengo, G., Pan, J., Heuberger, M., & Israelachvili, J. N. (1998). Temperature and time effects on the “adhesion dynamics” of poly (butyl methacrylate)(PBMA) surfaces. *Langmuir*, 14(14), 3873-3881.
- [89] Wahl, K. J., Asif, S. A. S., Greenwood, J. A., & Johnson, K. L. (2006). Oscillating adhesive contacts between micron-scale tips and compliant polymers. *Journal of colloid and interface science*, 296(1), 178-188.
- [90] Ebenstein, D. M., & Wahl, K. J. (2006). A comparison of JKR-based methods to analyze quasi-static and dynamic indentation force curves. *Journal of colloid and interface science*, 298(2), 652-662.
- [91] Chopin, J., Villey, R., Yarusso, D., Barthel, E., Creton, C., & Ciccotti, M. (2018). Non-linear viscoelastic modeling of adhesive failure for polyacrylate pressure-sensitive adhesives. *Macromolecules*, 51(21), 8605-8610.
- [92] Creton, C., Hooker, J., & Shull, K. R. (2001). Bulk and interfacial contributions to the debonding mechanisms of soft adhesives: Extension to large strains. *Langmuir*, 17(16), 4948-4954.